Fully Integrated Active Quenching Circuit Driving Custom-Technology SPADs With 6.2 ns Dead Time

Francesco Ceccarelli, Giulia Acconcia, Angelo Gulinatti, *Member, IEEE*, Massimo Ghioni, *Senior Member, IEEE*, Ivan Rech, *Senior Member, IEEE*

***Abstract*—The minimization of the dead time necessary for the operation of a single-photon avalanche diode (SPAD) plays a crucial role in many demanding single-photon applications. Among these, it is worth mentioning the implementation of airborne light detection and ranging (LIDAR) systems exploited to scan the terrain topography through semiporous obscurations. In this letter, we present the development and the experimental characterization of a fully integrated active quenching circuit (AQC) able to drive custom-technology SPADs with a dead time as low as 6.2 ns, corresponding to a maximum photon count rate of more than 160 Mcps. Thanks to the use of a high-voltage CMOS fabrication technology, the circuit is able to operate also SPADs that require an excess bias of few tens of Volts, like the recently developed red-enhanced SPAD (RE-SPAD), up to a maximum photon count rate of 100 Mcps.**

***Index Terms*—Single-photon avalanche diode (SPAD), red-enhanced SPAD (RE-SPAD), active quenching circuit (AQC), single-photon counting (SPC), dead time.**

I. Introduction

SINGLE-PHOTON avalanche diodes (SPADs) are photodetectors in which individual photons produce macroscopic current pulses that can be counted in order to measure the intensity of an optical signal: this approach is usually referred to as Geiger mode operation.

In the last years, a widespread interest in SPADs has been grown in several scientific and industrial applications, such as quantum cryptography [1], single-molecule fluorescence spectroscopy [2], light detection and ranging (LIDAR) [3] and many others. In particular, the use of SPADs in LIDAR systems has been widely investigated as a valuable alternative to analog avalanche photodiodes (APDs), in which the output current is proportional to the incident optical power. The use of single-photon detectors in LIDAR systems is driven by the prospect of providing a range measurement by using only one detected photon per flash as opposed to hundreds of photons required by traditional linear LIDAR [4]. Indeed, such a feature enables the measurement of significantly longer ranges, the reduction of the optical power of the laser source and the implementation of high frame rate 3D imaging systems, thanks to the possibility of replacing a single detector that scans the entire field of view with a SPAD array [5]. However, a single-photon LIDAR system has to cope also with some disadvantages that intrinsically affect the Geiger mode operation: as an example, each time that a photon is detected, the SPAD can not record another photon arrival in a given time span, usually referred to as dead time. Therefore, in the case of airborne LIDAR altimeters that scan the terrain topography through a semiporous obscuration (e.g. tree canopies, ground fog, clouds, etc.) the first photons that are reflected can mask the photons actually scattered by the terrain. As a consequence, a dead time in the nanosecond range is mandatory to record the photons reflected by surfaces having a distance of few meters [6]. A minimal dead time is also of paramount importance in presence of a strong background (e.g. during daylight operations), when the LIDAR receiver can fall into paralyzation due to the high rate of photon detections [7].

Today the best results reported in the literature in terms of SPAD dead time have been achieved by exploiting standard CMOS fabrication processes [8], [9], thanks to the possibility of integrating both the detector and the quenching electronics on the same chip, thus minimizing the parasitics that affect the quench and reset transients. However, this approach provides only a limited set of degrees of freedom for the design of the SPAD, thus the attainable performance are often not optimal. As an example, Niclass et al. [9] reported a very short dead time of 6 ns; however, this result was attained along with a peak photon detection efficiency (PDE) of only 20% at 470 nm (with no further data for the longer wavelengths, that are of the utmost interest in LIDAR applications [3]).

On the other hand, it has been demonstrated that the use of a purposely developed fabrication process (i.e. a custom technology [10]) allows the full optimization of the SPAD performance, although this choice makes the integration of the quenching electronics in the detector chip not practical, forcing the designer to fabricate the SPADs and the auxiliary electronics in separate dies. Despite the inevitable increase in parasitics, this approach produced excellent results: indeed we have already demonstrated that a thin SPAD [10] having a peak detection efficiency of 50% at 550 nm (about 15% at 800 nm) can be operated by an external active quenching circuit (AQC) with a dead time as low as 8.3 ns [11]. This result is even more remarkable considering that the aforementioned thin SPAD has an active area with a diameter as large as 50 μm, while both Eisele et al. [8] and Niclass et al. [9] presented their results for a SPAD having a diameter of only 8 μm.

In this letter, we present a fully integrated AQC able to drive an external thin SPAD with a dead time as low as 6.2 ns, the best value reported so far for a custom-technology

This work was performed in part at the Cornell NanoScale Science & Technology Facility, a member of the National Nanotechnology Coordinated Infrastructure, which is supported by the National Science Foundation under Grant ECCS-1542081.

The authors are with the Dipartimento di Elettronica, Informazione e Bioingegneria, Politecnico di Milano, 20133 Milano, Italy (e-mail: giulia.acconcia@polimi.it).

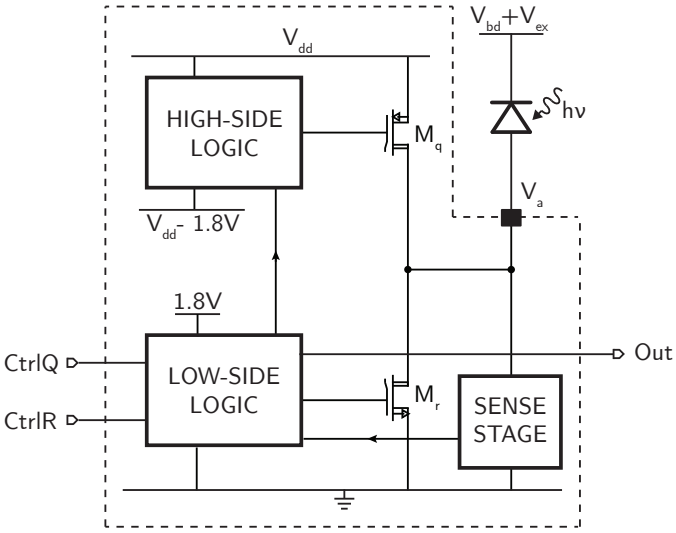

Fig. 1. Simplified representation of the AQC internal architecture.

SPAD. The result of the experimental characterization fully demonstrates that the AQC is able to operate both the thin and the red-enhanced SPAD (RE-SPAD) [12], a custom-technology detector that provides a PDE as high as 40% at 800 nm when biased at 20 V over the breakdown voltage. In particular, the circuit allowed us to demonstrate that a RE-SPAD can attain a dead time as low as 10 ns, a value that represents the record among the SPADs featuring red-enhanced sensitivity [13], [14].

II. AQC ARCHITECTURE

The new AQC was fabricated by employing the high-voltage 0.18 µm CMOS technology from Austriamicrosystems (ams H18). The architecture of the circuit (Fig. 1) is the same we described in [15] and that was used to demonstrate a dead time of 10 ns at room temperature [16] and a dead time of 8.3 ns at -20 °C [11]. Upon the detection of a photon, the SPAD avalanche current is read out by the sense stage that promptly provides an initial passive quenching of the avalanche and activates the logic circuits. Then, the quenching phase is actively completed by the high-voltage p-type MOSFET M_q that is controlled by the high-side logic block. Finally, the low-side logic block is responsible for driving the high-voltage n-type MOSFET M_r, used to reset the SPAD, and provides an output pulse Out synchronous with the photon detection.

The AQC features a few control input pins to regulate its behavior: above all, the voltages applied to $CtrlQ$ and $CtrlR$ adjust two independent monostable circuits that set the duration of the quenching and the reset phase. To minimize the dead time, the circuit presented in this paper features two main differences with respect to [16]. First of all, the two monostables that set the duration of the quench and the reset were modified to reduce the minimum duration of these phases. To this aim, maintaining the structure reported in [16], the aspect ratio of the p-MOSFET was increased up to 2 µm / 0.5 µm. Secondly, also the aspect ratio of the transistors M_q and M_r was increased to reduce the time span needed to apply the quenching/reset pulses. Now M_q features a W/L as large as 400 µm / 0.2 µm while the aspect ratio of M_r is 650 µm / 0.2 µm. The drivers of these two MOSFETs, each one consisting in a cascade of an even number of inverters with progressive gate sizes, were designed to drive the high gate capacitance of M_q and M_r, respectively 2.7 pF and 4 pF.

The AQC, without pads, features an overall area of 364 µm × 90 µm.

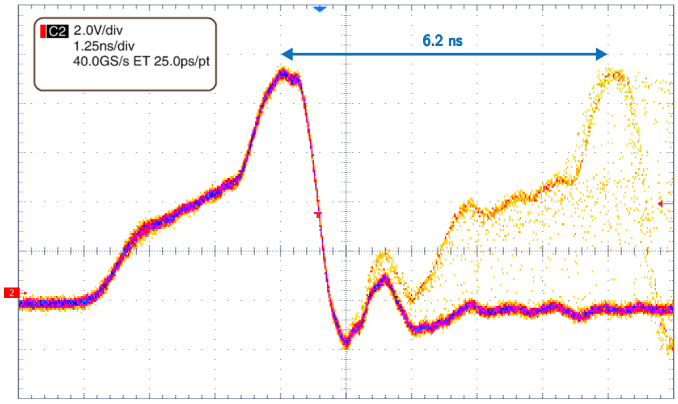

Fig. 2. Waveform of the anode voltage V_a for a thin SPAD operated with the presented AQC.

III. EXPERIMENTAL RESULTS

After the fabrication, the AQC was experimentally characterized with both thin and red-enhanced SPADs. In the following sections we report the waveform recorded at the SPAD anode terminal after a photon detection, in order to show that the circuit can operate custom-technology SPADs with a dead time down to the nanosecond range. However, since the afterpulsing performance of the detector can be negatively affected by the operation with such a short dead time, we decided also to report the afterpulsing probability of our SPADs, when operated by the presented AQC.

A. Thin SPAD

Firstly, the AQC was tested with a custom-technology thin SPAD (active area diameter $D = 50$ µm and breakdown voltage $V_{bd} = 36.1$ V) in order to characterize the minimum dead time achievable by the circuit. Both the AQC and the SPAD were mounted on a printed circuit board (PCB), on which $CtrlQ$ and $CtrlR$ were chosen in order to achieve the maximum speed. The waveform of the anode voltage V_a was read using a fast oscilloscope (Tektronix TDS7404B) through an on-board AC coupling ($C = 1$ pF) in order to limit the increase of the total capacitance driven by the AQC. The detector was operated in dark condition, with an excess bias V_{ex} = 5 V.

The result is showed in Fig. 2: as soon as the photon arrives the passive quenching starts; after 3 ns, the quench transistor M_q is activated by the high-side logic and the quenching operation is completed by driving the anode voltage V_a up to $V_{dd} = 9$ V in only 1 ns. Finally, the reset transistor M_r drives V_a to ground in a time span as low as 2.2 ns. Therefore, the minimum distance between two consecutive pulses is as

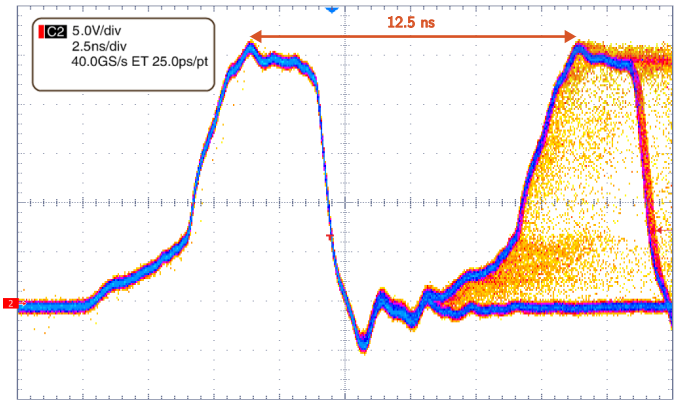

Fig. 3. Waveform of the anode voltage V_a for a RE-SPAD operated with the presented AQC.

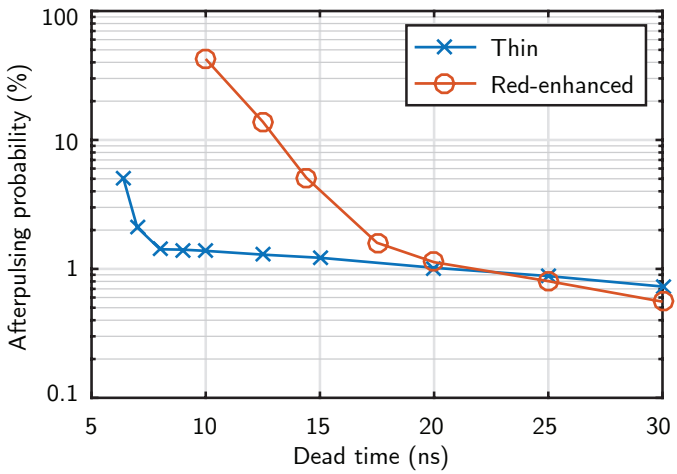

Fig. 4. Afterpulsing probability as a function of the dead time. Results for both thin and red-enhanced SPADs are reported.

low as 6.2 ns, corresponding to a maximum count rate of more than 160 Mcps, that we verified by illuminating the detector up to the oscillation condition.

A short dead time is useful not only to avoid photon masking or paralyzation, but also to remarkably increase the speed of time-correlated single-photon counting (TCSPC) measurements [17]: indeed, the dead time can be finely tuned to match the period of the excitation laser, thus allowing the recording of TCSPC histograms with no pile-up distortion, even at detection rates higher than 5% [17]. The feasibility of the implementation of high-speed TCSPC systems based on this AQC is also demonstrated by the very fast reset transition that the circuit provides, a requirement of paramount importance in order to minimize the photon detection probability during the reset phase. Finally, it is worth noting also that these results were attained by using $V_{dd} = 9$ V, a value that allows the new AQC to correctly quench the avalanche even with an excess bias greater than 5 V. This possibility is very important in all those applications in which a higher PDE is crucial or in which the noise is limited by the background.

B. Red-enhanced SPAD

Secondly, we took advantage of the same setup in order to characterize the operation of the new AQC with a RE-SPAD. The detector we used was the one already exploited in [18] (active area diameter $D = 50$ µm and breakdown voltage $V_{bd} = 41.5$ V) in order to demonstrate the best timing performance to date among all the SPADs with red-enhanced sensitivity. Indeed, this detector was designed with great attention at the minimization of the capacitive load on the anode terminal, a feature that is of paramount importance not only to improve the timing performance of the RE-SPAD, but also to minimize the achievable dead time.

The waveform acquired at the anode terminal is reported in Fig. 3 for $V_{ex} = 20$ V and $V_{dd} = 25$ V. As already discussed for Fig. 2, the three phases of the quenching operation are clearly appreciable. However, in this case a strong afterpulsing prevented the correct operation with $CtrlQ$ and $CtrlR$ configured to achieve the minimum dead time. Therefore, we decided to set the total dead time at 12.5 ns: with this configuration the afterpulsing probability is still high, as clearly visible in Fig. 3 by noting that the second pulse has an intensity similar to the pulse on which the oscilloscope is triggered; however, the operation of the detector is not impaired and the AQC is able to correctly quench and reset the SPAD.

These results open the way for the exploitation of the RE-SPAD in high-speed TCSPC applications [17] in which an 80-MHz repetition rate laser is employed. Moreover, all these measurements were performed with the substrate terminal fixed at a given voltage, as required by SPAD arrays in order to limit the electrical crosstalk among the pixels [18]. This means that the AQC is suitable also for the implementation of detection systems based on RE-SPAD arrays, that can be exploited as LIDAR receivers or high-speed TCSPC imagers.

C. Afterpulsing

Finally, the afterpulsing probability of both the SPADs was characterized by exploiting the same procedure used in [11]. After a time-stamping measurement, the autocorrelation function (ACF) of the data stream composed by the arrival times of each pulse is calculated. The ACF represents the average count rate as a function of the delay τ from a generic pulse and allows the computation of F_{ap}, defined as the ratio between the total number of correlated events N_c and the total number of uncorrelated events N_{uc}:

$$F_{ap} = \frac{N_c}{N_{uc}} = \int_{T_{dead}}^{+\infty} [ACF(\tau) - n_{uc}] d\tau, \qquad (1)$$

where n_{uc} is the average count rate due to the uncorrelated events (in our case the dark counts due to thermal generation). If $F_{ap} << 1$, this value represents a good estimation of the afterpulsing probability P_{ap}. Otherwise, N_c keeps in account also the afterpulses that originate from other afterpulsing events, that are correlated in time to the primary event and thus can not be distinguished from the first order afterpulsing. Mathematically speaking, the number of afterpulses of order n is $N_{uc}P_{ap}^n$. Therefore:

$$F_{ap} = P_{ap} + P_{ap}^2 + P_{ap}^3 + ... = \sum_{n=1}^{+\infty} P_{ap}^n = \frac{P_{ap}}{1 - P_{ap}}. \qquad (2)$$

By solving Eq. 2 for P_{ap} it is possible to obtain:

$$P_{ap} = \frac{F_{ap}}{1 + F_{ap}}. \quad (3)$$

To measure the ACF we used the same PCB of the previous sections, with the time-stamper connected to the AQC output. As we did not need to monitor the anode waveform any longer, we removed the oscilloscope probe and connected the AQC to the SPAD anode with a direct wire-bonding. This configuration allows a further reduction of the capacitive load driven by the circuit, thus minimizing the avalanche charge flowing in the SPAD and, as a consequence, reducing the number of afterpulsing events. Thanks to this choice we managed to correctly operate the RE-SPAD with a dead time down to 10 ns, pushing the maximum achievable count rate up to 100 Mcps.

The experimental results are summarized in Fig. 4, where the afterpulsing probability P_{ap} of both the SPADs is reported as a function of the dead time T_{dead}, that we swept by acting on the $CtrlQ$ terminal. For the thin SPAD, the afterpulsing probability is lower than 1.4% down to $T_{dead} = 8$ ns. A further reduction of the dead time results in a steep increase of the afterpulsing probability, that, nevertheless, remains lower than 5% even when the SPAD is operated at 6.2 ns. These values demonstrate that the exploitation of a thin SPAD, operated by the presented AQC, is feasible in the applications. On the other hand, the afterpulsing probability of the RE-SPAD remains below a few percent down to $T_{dead} = 14$ ns. A further reduction of the dead time results in a strong afterpulsing, that peaks at 42% when the SPAD is operated at 10 ns. This value is clearly too high for most of the applications. In the future we will investigate the reasons for such a steep increase in the afterpulsing probability and we will work at the design and fabrication of a RE-SPAD with an afterpulsing probability comparable with the thin SPAD also at short dead times.

IV. Conclusion

The exploitation of a custom technology for the SPAD fabrication allows the achievement of an excellent performance, but there exists a price to pay: the integration of both detector and quenching electronics in the same chip is not easily feasible, forcing the designer to fabricate them in separate chips and thus making the effect of the electrical parasitics not always negligible. Nevertheless, in this letter we have demonstrated that this drawback does not prevent the operation of a thin SPAD with a dead time as low as 6.2 ns, a value that represents the state of the art among all the custom-technology SPADs and that is comparable to the 5.4 ns dead time reported for an 8 µm CMOS SPAD in [8]. In addition, the experimental characterization has also showed that this dead time can be attained along with an afterpulsing probability in the percent range, demonstrating that the circuit can meet the demanding requirements of the high-performance applications.

Thanks to the use of a high-voltage CMOS technology, the presented AQC is also compatible with SPADs that need a high excess bias to provide high PDE in the red and near infrared range. In particular, we have showed that a RE-SPAD can be operated with a dead time down to 10 ns. This result compares favorably with the 20 ns dead time reported in [13], [14] and, to the best of our knowledge, represents the best value reported so far for a SPAD with red-enhanced sensitivity.

Acknowledgement

The authors wish to acknowledge P. Maccagnani (Istituto per la Microelettronica e Microsistemi - Consiglio Nazionale delle Ricerche, sez. Bologna) for the fabrication of the thin SPAD. The RE-SPAD employed in this work was fabricated by the authors at the Cornell NanoScale Science & Technology Facility, a member of the National Nanotechnology Coordinated Infrastructure.

References

[1] K. J. Gordon *et al.*, "A short wavelength gigahertz clocked fiber-optic quantum key distribution system," *IEEE J. Quantum Electron.*, vol. 40, no. 7, pp. 900–908, Jul. 2004.

[2] X. Michalet *et al.*, "Silicon photon-counting avalanche diodes for single-molecule fluorescence spectroscopy," *IEEE J. Sel. Topics Quantum Electron.*, vol. 20, no. 6, pp. 248–267, Nov. 2014.

[3] G. S. Buller *et al.*, "Ranging and three-dimensional imaging using time-correlated single-photon counting and point-by-point acquisition," *IEEE J. Sel. Topics Quantum Electron.*, vol. 13, no. 4, pp. 1006–1015, Jul. 2007.

[4] M. A. Krainak *et al.*, "Comparison of linear-mode avalanche photodiode lidar receivers for use at one-micron wavelength," in *Proc. SPIE*, vol. 7681, Apr. 2010, p. 76810Y.

[5] C. Niclass *et al.*, "A 0.18-µm CMOS SoC for a 100-m-range 10-frame/s 200×96-pixel time-of-flight depth sensor," *IEEE J. Solid-State Circuits*, vol. 49, no. 1, pp. 315–330, Jan. 2014.

[6] J. J. Degnan, "Scanning, multibeam, single photon lidars for rapid, large scale, high resolution, topographic and bathymetric mapping," *Remote Sens.*, vol. 8, no. 11, p. 958, Nov. 2016.

[7] ——, "Impact of receiver deadtime on photon-counting SLR and altimetry during daylight operations," in *Proc. IWLR*, Oct. 2008, pp. 339–346.

[8] A. Eisele *et al.*, "185 MHz count rate, 139 dB dynamic range single-photon avalanche diode with active quenching circuit in 130 nm CMOS technology," in *Proc. IISW*, Jun. 2011, pp. 6–8.

[9] C. Niclass *et al.*, "A miniature actively recharged single-photon detector free of afterpulsing effects with 6ns dead time in a 0.18µm CMOS technology," in *Proc. IEDM*, Dec. 2010, pp. 14.3.1–14.3.4.

[10] M. Ghioni *et al.*, "Progress in silicon single-photon avalanche diodes," *IEEE J. Sel. Topics Quantum Electron.*, vol. 13, no. 4, pp. 852–862, Jul. 2007.

[11] F. Ceccarelli *et al.*, "152-db dynamic range with a large-area custom-technology single-photon avalanche diode," *IEEE Photon. Technol. Lett.*, vol. 30, no. 4, pp. 391–394, Feb. 2018.

[12] A. Gulinatti *et al.*, "New silicon SPAD technology for enhanced red-sensitivity, high-resolution timing and system integration," *J. Mod. Opt.*, vol. 59, no. 17, pp. 1489–1499, Jul. 2012.

[13] M. Stipčević *et al.*, "Characterization of a novel avalanche photodiode for single photon detection in VIS-NIR range," *Opt. Express*, vol. 18, no. 16, pp. 17 448–17 459, Aug. 2010.

[14] (2017) Excelitas SPCM-AQRH series datasheet. [Online]. Available: http://www.excelitas.com/Downloads/DTS_SPCM-AQRH.pdf

[15] G. Acconcia *et al.*, "High-voltage integrated active quenching circuit for single photon count rate up to 80 Mcounts/s," *Opt. Express*, vol. 24, no. 16, pp. 17 819–17 831, Aug. 2016.

[16] ——, "Note: Fully integrated active quenching circuit achieving 100 MHz count rate with custom technology single photon avalanche diodes," *Rev. Sci. Instrum.*, vol. 88, no. 2, p. 026103, Feb. 2017.

[17] A. Cominelli *et al.*, "High-speed and low-distortion solution for time-correlated single photon counting measurements: A theoretical analysis," *Rev. Sci. Instrum.*, vol. 88, no. 12, p. 123701, Dec. 2017.

[18] F. Ceccarelli *et al.*, "83-ps timing jitter with a red-enhanced SPAD and a fully integrated front end circuit," *IEEE Photon. Technol. Lett.*, vol. 30, no. 19, pp. 1727–1730, Oct. 2018.